Jurnal Pendidikan Teknologi Kejuruan, Vol. 6, No. 1, pp. 1-8, February 2023
e-ISSN 2621-1548; p-ISSN 2621-3273

Synthesis optimization of cathode precursor $Ni_{0,5}$ $Mn_{0,4}$ $Co_0.1$ $(OH)_2$ with coprecipitation method

Muhammad Abdul Razak* **and Anne Zulfia**

Department of Metallurgy and Materials Engineering, Universitas Indonesia, **Indonesia**

*Corresponding Author: marazak.97@gmail.com
Received 12th Jan 2023; 1st Revision 18th Jan 2023; 2nd Revision 2nd Feb 2023; Accepted 18th Feb 2023

Cite this https://doi.org/10.24036/jptk.v6i1.30523

Abstract: The use of conventional fuels such from fossils sourced is non-renewable energy, which makes this energy source less environmentally friendly. The battery that is nowadays used widely is the Lithium-Ion type with variations in the type of electrode. Electrodes have an important role in battery performance, especially at the cathode. Predecessor cathode types such as $LiCoO_2$, LiMnO, and LiNiCo have various disadvantages due to their dangerous nature, insufficient capacity, and poor stability. NMC cathode (NiMnCo), in this case, NMC541 is presented to overcome these deficiencies. The process of making NMC541 cathode can be done by various synthesis methods, one of which is Co-precipitation. The synthesis parameter directly influences the performance of the cathode precursor produced, especially on its microstructure. For that, we try to optimize the synthesis parameters, such as Stirring Speed, and Aging time. The result said that samples with 900 RPM stirring speed give the best product precursor along to their small size particle and good conductivity. Meanwhile, Aging co-precipitation doesn't significantly affect coprecipitation precursor products.

Keywords: NMC541; Co-precipitation; Aging; Steering speed

1. Introduction

The source of electric power requires a device to generate, store and transmit electrical energy. Batteries are one of the devices that are used to store electrical energy with various types of constituent components. Batteries consist of several main components that have their respective functions, namely the cathode, anode, and electrolyte. Lithium Ion batteries are widely used in vehicles powered by electricity because they have the advantages of high energy density and strength and can be used at relatively high temperatures, long life cycles, and low self-discharge rates.

Among the uses of lithium ion Batteries, many types of cathode components have been used and developed through research by previous experts. Some examples of the use of cathodes, namely, $LiCoO_2$, have the lack of toxic properties of its cobalt (Liu et al., 2022). On another side, the use of $LiNiO_2$ cathodes has the disadvantage of being difficult to synthesize and is also known for its poor ability to charge-discharge due to two main drawbacks, namely its non-stoichiometric tendency due to the displacement of Li/Ni cations during the synthesis process and its structural instability during lithium intercalation/deintercalation processes (Liang et al., 2014). Whereas the $LiMnO_2$ cathode has a large enough capacitance, however during the charge-discharge process, the spherical structure of the $LiMnO_2$ constituent is very easy to change into a Spinel structure causing a decrease in storage capacity.

Here comes a new type of cathode $LiNi_{1-x-y}Co_xMn_y$ (LiNMC) tries to combine the several types of cathodes above with various advantages and disadvantages, which are expected to form a cathode that can store a lot of energy, and low production costs, is safe and has a long service life (Zhang et al., 2012).

Various researchers have conducted research subjected to the type of synthesis carried out on the LiNMC cathode. To find more optimal results, it is necessary to optimize the parameters that affect the synthesis process such as Steering speed and Aging time during the co-precipitation process. Stirring speed affects the formation of spherical particles. Increasing the speed of stirring can increase the collision between

particles and between particles and the walls of the vessel, which is useful for forming spherical particles that are uniform and homogeneous. Whereas in the Aging time variable, the time variation treatment can provide time for the particles to crystallize and disperse in parts and have their respective sizes (Jeong et al., 2016).

2. Methods

Synthesis Procedure

This research was conducted by making samples at each variable of stirring speed, and Aging time during co-precipitation synthesis using pH 11, to obtain NMC ratio results that are close to a 5:4:1 ratio, and a microstructural shape that is close to spherical. By testing the SEM microstructure, XRF, XRD and Conductivity testing using LCR, each specimen at a certain variable will be tested on its respective test equipment.

Sample preparation

Sample preparation was carried out by weighing $Ni(CH_3CO_2)_2{\cdot}4H_2O$, $Mn(CH_3CO_2)_2{\cdot}4H_2O$, and $Co(CH_3CO_2)_2{\cdot}4H_2O$ with a molarity ratio of 5:4:1. After the raw materials are weighed, each raw material will be dissolved with 50 ml of aquabidest for each raw material, then mixed with each of these solutions for 4 hours of stirring. The chelating agent solution is dissolved in a 1:1 ratio with the Transition Material (TM) solution. After all the solutions were stirred for 4 hours, the solutions were precipitated during the various settling times. After precipitation, the solution is filtered using filter paper, then dried using a vacuum oven for 3 hours at temperature of 100°C.

Sample characterization

The characterization of the sample was carried out by several tests, including XRF, XRD, SEM, and LCR. XRF testing is intended to determine the chemical content of a sample that is shot with X-ray gamma rays, which generates electron excitation at the core level to the excitation receiver. The XRF instrument used was Orbis Edax Ametek with 300 µm or 100 µm mono-capillary X-ray optics. SEM characterization was carried out to determine the shape of the grains resulting from the cathode synthesis of NMC541(OH)2, by using X-ray beams in a raster pattern over the entire surface of the sample, and the scattering of emitted secondary electrons will be recaptured by the detector. The SEM instrument used was Shimadzu XD-610 which was equipped with a target source of Cu Kα which was carried out at room temperature. XRD characterization was carried out with Cu Kα radiation ($\lambda = 1.5406$). XRD characterization was carried out to determine the chemical content formed from the sample which is described through diffraction patterns that have a distinctive shape. LCR meter is a measuring instrument that measures a quantity known as impedance. Impedance, expressed using the Z notation, denotes the resistance to the flow of AC current. LCR testing is carried out by providing frequencies from the range of 42 Hz to 1 GHz. The LCR instrument used is Hioki IM3533.

3. Results

Characterization with the SEM method was carried out with 2 magnifications, which were 1000x, 5000x, and 10.000x. This is done to determine the effect of testing the synthesis variables on the primary particles and secondary particles formed. From the secondary particles formed, grain size calculations were carried out using the image processing software.

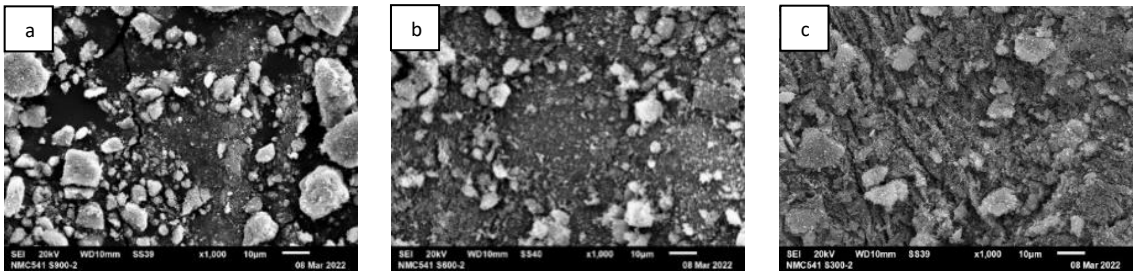

Figure 1. SEM test results with a magnification of 1000x at variable stirring speed: (a) Sample S900, (b) Sample S600, (c) Sample S300

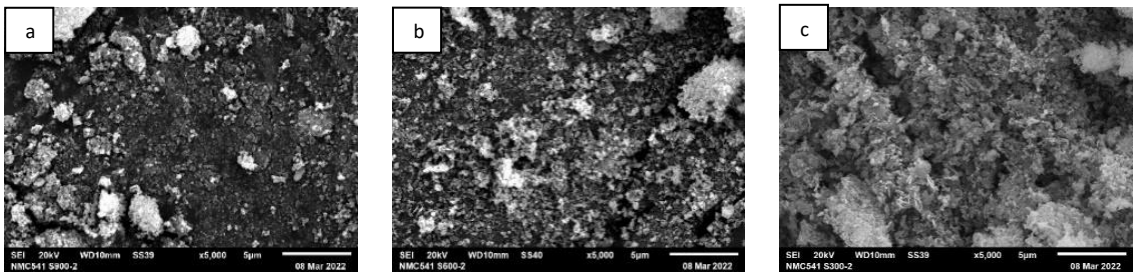

Figure 2. SEM test results Magnification 5000x variable stirring speed: (a) Sample S900, (b) Sample S600, (c) Sample S300

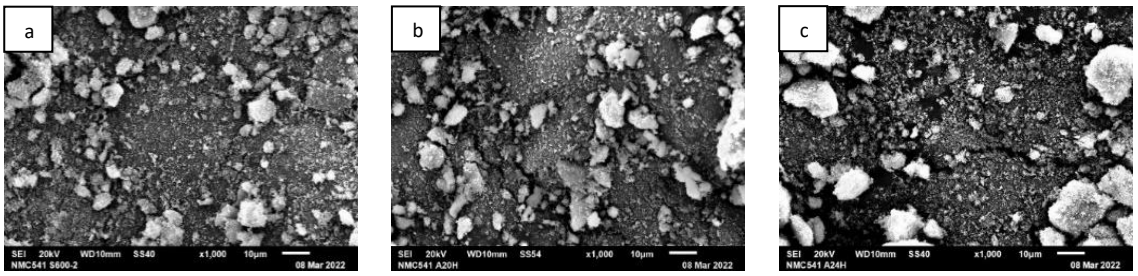

Figure 3. SEM test results at 1000x magnification at the aging time variable: (a) Sample A16h (b) Sample A20h, (c) Sample A24h

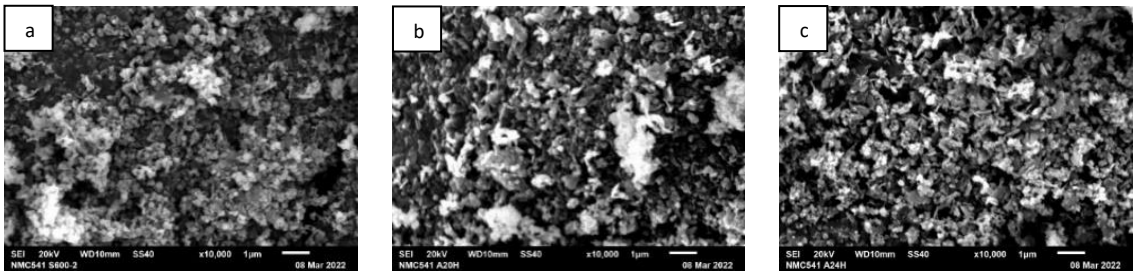

Figure 4. SEM test results at 10,000x magnification at the aging time variable: (a) Sample A16h (b) Sample A20h, (c) Sample A24h

The characterization of XRD was carried out at a theta angle of 10-80° with a Cu material anode. The results of the formed diffraction which describes the chemical content of the sample are then analyzed using the Highscore plus software.

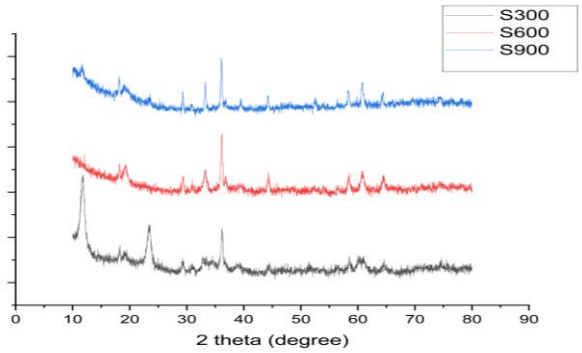

Figure 5. XRD test comparison of stirring speed variable

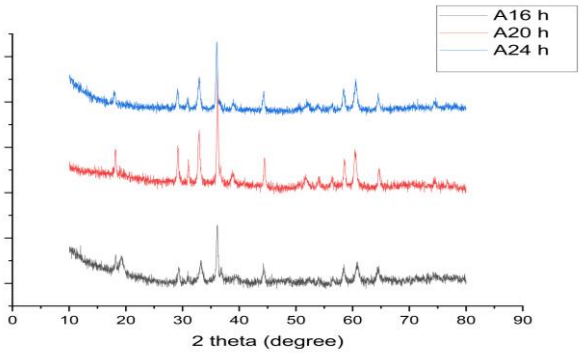

Figure 6. XRD test comparison of aging time variable

The LCR test is intended to determine the conductance of the cathode material which has been pelleted and tested at a frequency of 42 Hz - 1 GHz. The conductance calculation is carried out on the Plateau area which is shown in orange color.

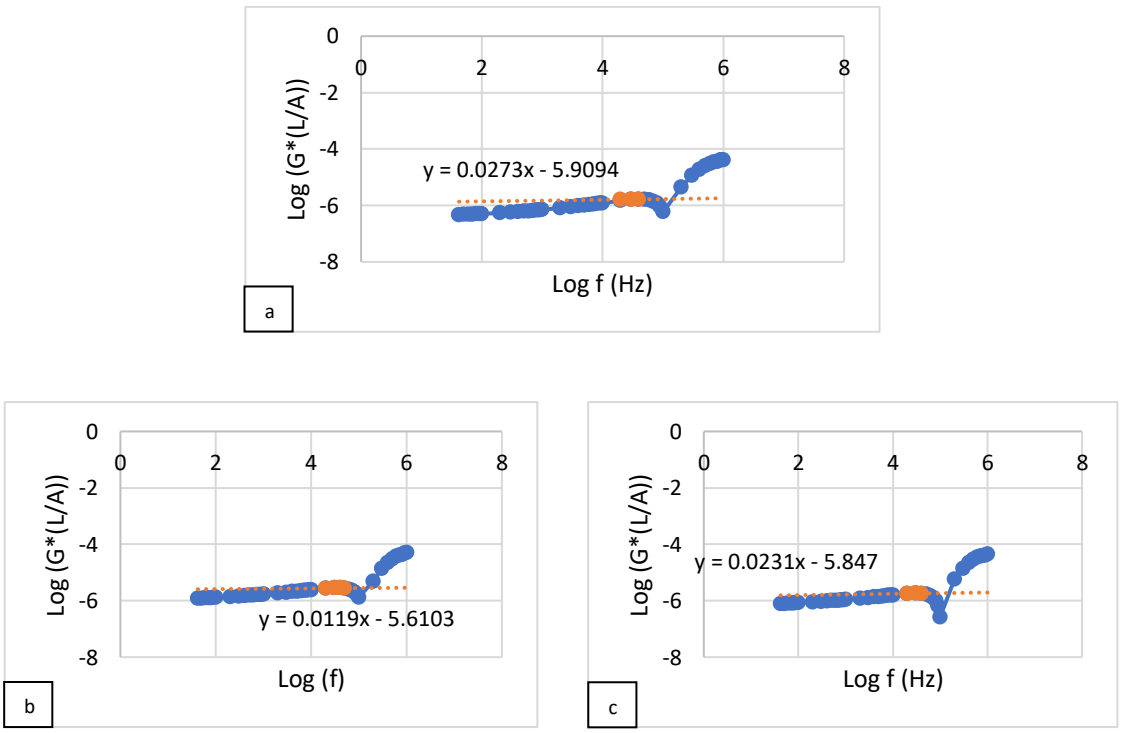

Figure 7. Aging time variable conductivity test: (a) Sample A16h, (b) Sample A20h, and (c) Sample A24h

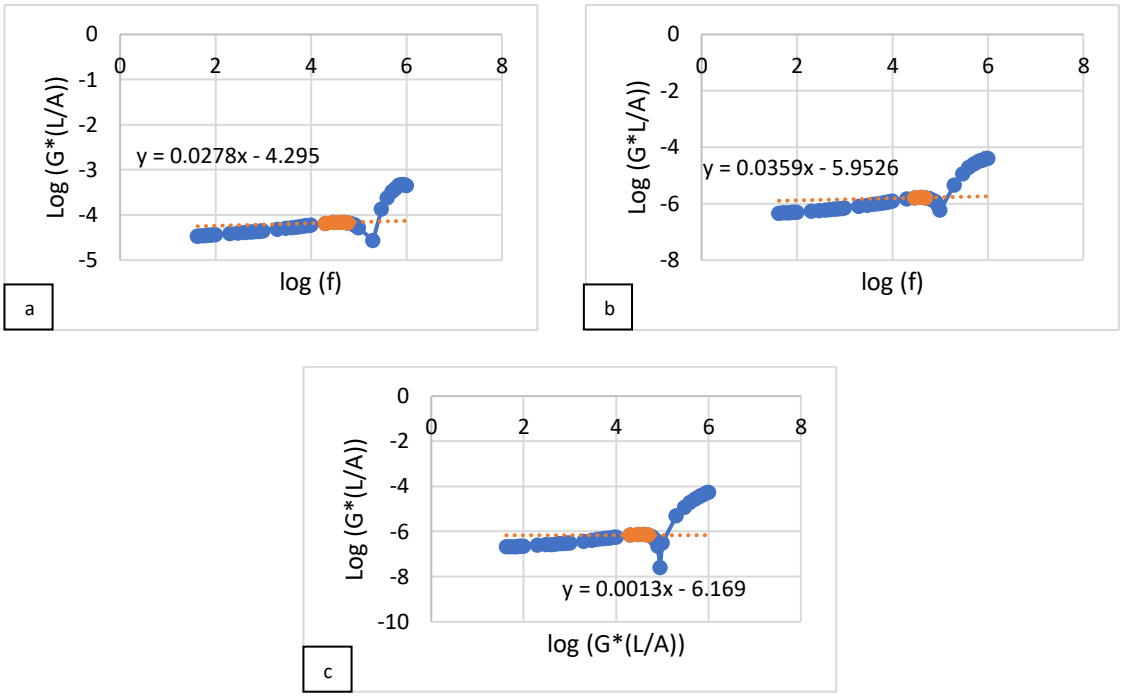

Figure 8. Conductivity test with variable speed of stirring: (a) Sample S900, (b) Sample S600, and (c) Sample S300

XRF testing is based on emitting X-rays to determine the chemical content formed in the sample. XRF testing will produce %Wt or %At data which is then calculated by dividing by the relative atoms of each chemical element so that the molarity of each chemical element is obtained, the molarity results will be calculated as a ratio.

Table 1. Molar ratio of all variable

%At	Ni	Mn	Co
S300	9,48	79,26	11,26
S600	6,04	81,74	12,22
S900	8,92	79	12,08
A16h	6,04	81,74	12,22
A24h	13,07	75,2	11,73
A20H	12,52	75,66	11,82

4. Discussion

SEM results

Based on the results of the 5000x magnification SEM test (Figure 2), it can be seen that in general, it Is figured out that the primary particles of the sample, that along with the increase in speed, the primary particles will tend to be spherical in shape. In the S300 sample, the primary particles formed as sphere-like shape in some areas but were still contaminated in some areas that had needle-like particles. In the S600 sample, the primary particles form a sphere particle and are more generally distributed compared to the S300 sample and in the S900 sample the primary particles form a spherical shape with a more general distribution of sizes compared to the S600 sample.

Based on the SEM test on the three aging samples (Figure 4) with a magnification of 10,000x, it can be seen that the differences in the shape of the primary particles. In sample A16h, the primary particle shape is

rounded and spread generally with a nearly uniform size. Whereas A20h has a sphere-like primary particle shape but there are several needle-like particles, besides that the primary particle size is larger when compared to the primary particle sample A16h. Meanwhile, the A24h sample has primary particles that are more like needles and also have a larger particle size.

Based on the results of the 1000x magnification SEM test (Figure 4.1), in general, it will describe the secondary particles of the sample, that along with increasing speed, secondary particles will tend to be spherical in shape, have a smoother surface and have a more uniform size. Stirring speed can also affect the secondary particle size. In the S300 sample, it is illustrated that the secondary particles are not spherical in shape, have a rough surface, and do not have a uniform shape. If the speed of stirring is increased to S600, then it figures out the secondary particles that are already directed to a spherical shape, have a smooth surface but the secondary particle size that is not very uniform. As the speed of stirring at S900 increases, the distribution of secondary particle sizes becomes more uniform, the surface is smoother and the shape of the secondary particles is more like a spherical.

Based on the results of the SEM test of the three samples at 1000x magnification (Figure 3), it can be seen that the secondary particles of the three samples at the time of aging have a shape that tends not to be spherical. The difference in shape between the three samples shows that sample A16h has a shape that tends to be spherical but has a secondary particle size that is not very uniform. The A20h sample also has a secondary particle shape that is not very uniform, it tends to be the same as the A16h sample. When compared with the SEM results, sample A24h has a larger secondary particle size and tends to be more non-uniform in its secondary particle size.

XRD results

From Figure 5, it can be seen that the diffraction formed from the variable of the stirring speed samples has a pattern that resembles α-NiOH in the S300 diffraction sample and β-NiOH in the S900 diffraction (Portemer et al., 1992). Whereas in Sample S600 there is a transition between α to β-NiOH but more like β-NiOH. The diffraction pattern depicted on the S300 sample resembles α-NiOH with a P-3m1 space group. Along with increasing the stirring speed, in the S600 and S900 samples the peaks formed resembled β-NiOH which had a P-3m1 space group with increasingly high and sharp peak shapes depicting a smaller crystalline form. This was proven in the S300 sample, which described a lower intensity and had impurities, this was caused by the precursor redeposition rate being too fast during the crystallization process (Voorhees, 1985). Transition metals and hydroxide precipitators collide with each other through the thermal motion to form smaller crystal nuclei. Since the surface energy is much less than that of the larger particles, the smaller grains in the ammonia and sodium hydroxide solutions will be dissolved to reach the energy balance of the entire system. While all the hydroxides are in a supersaturated state, they will be precipitated back on the larger grains by secondary nucleation.

Based on the results of the XRD test on the Aging time sample (Figure 6), it can be seen that the diffraction formed has a pattern similar to β-NiOH (space group I41/amd) in the diffraction of each sample. In each sample there is no significant difference in the diffraction intensity. Synthesis on hydroxide precursors can produce different structures such as combinations of Ni(OH) and Mn(OH) in α and β phases, especially when synthesizing precursors with high manganese content. However, the phase that is most likely to occur is β, because it produces an impurity and defect-free structure (El Mofid et al., 2014). Mn2O4 is formed because, in $Mn(OH)_2$, Mn^{2+} can easily be oxidized to become Mn^{3+} and then separated in the form of a mixed hydroxide. With the formation of Mn2O4 resulting from the oxidation of Mn^{2+} confirms that the precursor formed is $TM(OH)_2$ not TMOOH. The peak at an angle of 2θ 36° has a not too significant difference in intensity, so it can be said that the variation in the aging time of 16-24 hours does not have a significant effect on the co-precipitation synthesis process.

LCR Result

From the conductivity (S) test performed, it can be calculated using following equation:

$$y = mx + a \quad (1)$$

$$S = 10\text{^}a \quad (2)$$

so that a comparison graph between frequency and conductivity is obtained, which is taken from the Plateau area (orange colored) with the following calculation results:

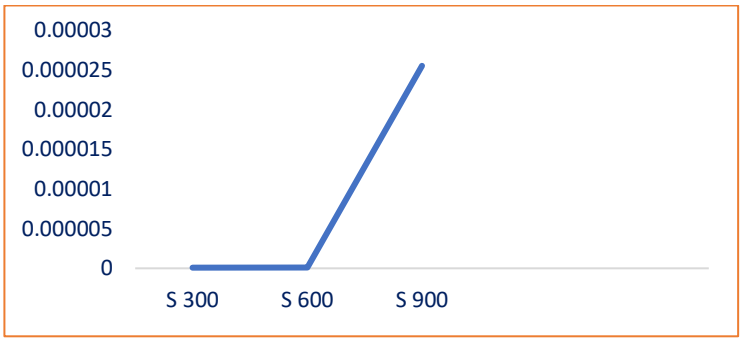

Figure 9. Comparison graph of Stirring speed variable

From the conductance logarithmic calculation above, the effect of increasing stirring speed will form a sample that has better conductivity. This confirms the microscopic shape of the spherical grains and the smaller the particle size, the better the conductivity.

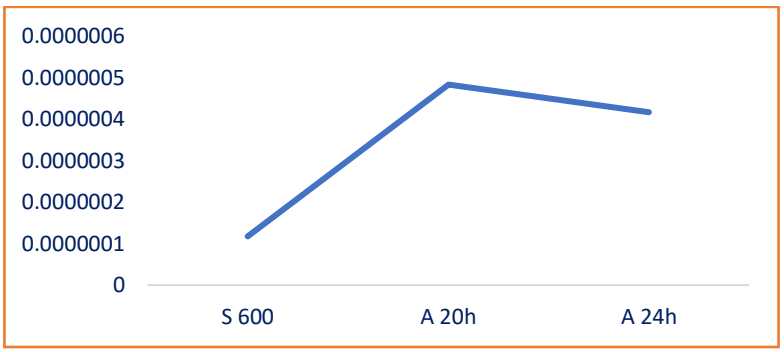

Figure 10. comparison graph of Aging time variable

Based on the results of the conductivity calculation above, the effect of aging time is that the longer the aging time will increase the conductivity, although the increase is not significant. The best conductivity occurs in sample A20 h, this confirms that as the grain size decreases, it will provide better conductivity.

XRF result

From the molarity calculation above, it can be concluded that there is no sample that has the exact ratio of 5:4:1 (Ni:Mn:Co). However, from the three samples above, along with increasing the stirring speed, the mole ratio in the S900 sample approached the ratio of 5:4:1. Along with the addition of aging time, also the mole ratio is slightly closer to the ratio of 5:4:1. This still needs to be studied further whether the synthesis process is still incomplete or whether there is a change in the mole ratio during the synthesis process. This still needs to be studied further whether the synthesis process is still incomplete or whether there is a change in the mole ratio during the synthesis process.

Table 2. XRF result of all variable

Molar Ratio (mol)	Ni	Mn	Co
S900	0,477318	0,44787	0,074812
S300	0,094773	0,792529	0,112698
S600	0,060392	0,817365	0,122243
A16h	0,060392	0,817365	0,122243
A20h	0,125182	0,756532	0,118286
A24H	0,130744	0,751883	0,117373

5. Conclusion

From research carried out before, there will be some conclusion:

1. Variation of stirring speed has an influence on the results of the NMC541 coprecipitation synthesis, as the speed of stirring increases, the collisions that occur are more intense between the particles and the walls, and with the magnetic stirrer resulting in a more even, spherical shape, and smaller in size in the sample S900;
2. Aging time variation does not have a significant effect on the results of the synthesis of NMC541 co-precipitation. This is indicated by the resulting precursor which has primary particles resembling needles, non-uniform grain shapes, and grain sizes that increase with increasing aging time;
3. In both test variables, the stirring speed variable has a greater role in the results of the synthesis of the NMC541 precursor. This is indicated by the S900 sample which has better conductivity, smaller grain size, and XRF results that are closer to the mole ratio of 5:4:1.

References

El Mofid, W., Ivanov, S., & Bund, A. (2014). Effect of synthesis conditions and composition modification on the structural and electrochemical properties of layered transition metal oxide cathode materials. *Proceedings of 2014 International Renewable and Sustainable Energy Conference, IRSEC 2014*, *June 2018*, 626–630. https://doi.org/10.1109/IRSEC.2014.7059798

Jeong, Y., Kim, I., Yeon, J., Yan, N., Jeong, H., Ki, J., Ho, J., & Chul, J. (2016). Journal of Molecular Catalysis A : Chemical Effect of the aging time of the precipitate on the activity of Cu / ZnO catalysts for alcohol-assisted low temperature methanol synthesis. *"Journal of Molecular Catalysis. A, Chemical," 418–419*, 168–174. https://doi.org/10.1016/j.molcata.2016.03.044

Liang, L., Du, K., Peng, Z., Cao, Y., Duan, J., Jiang, J., & Hu, G. (2014). Co-precipitation synthesis of Ni0.6Co0.2Mn 0.2(OH)2 precursor and characterization of LiNi 0.6Co0.2Mn0.2O2 cathode material for secondary lithium batteries. *Electrochimica Acta*, *130*, 82–89. https://doi.org/10.1016/j.electacta.2014.02.100

Liu, J., Duan, Q., Qi, K., Liu, Y., Sun, J., Wang, Z., & Wang, Q. (2022). Capacity fading mechanisms and state of health prediction of commercial lithium-ion battery in total lifespan. *Journal of Energy Storage*, *46*, 103910. https://doi.org/https://doi.org/10.1016/j.est.2021.103910

Portemer, F., Delahaye-Vidal, A., & Figlarz, M. (1992). Characterization of Active Material Deposited at the Nickel Hydroxide Electrode by Electrochemical Impregnation. *Journal of The Electrochemical Society*, *139*(3), 671. https://doi.org/10.1149/1.2069283

Voorhees, P. W. (1985). The theory of Ostwald ripening. *Journal of Statistical Physics*, *38*(1), 231–252. https://doi.org/10.1007/BF01017860

Zhang, B., Li, L., & Zheng, J. (2012). Characterization of multiple metals (Cr, Mg) substituted LiNi0.8Co0.1Mn0.1O2 cathode materials for lithium ion battery. *Journal of Alloys and Compounds*, *520*, 190–194. https://doi.org/https://doi.org/10.1016/j.jallcom.2012.01.004